Osteoarthritis and Cartilage 22 (2014) 1639–1650

Osteoarthritis and Cartilage

Development and reliability of a multi-modality scoring system for evaluation of disease progression in pre-clinical models of osteoarthritis: celecoxib may possess disease-modifying properties

A. Panahifar †, J.L. Jaremko ‡ **, A.G. Tessier §, R.G. Lambert ‡, W.P. Maksymowych ||, B.G. Fallone § ¶ #, M.R. Doschak † †† *

† *Faculty of Pharmacy & Pharmaceutical Sciences, University of Alberta, Edmonton, Alberta, Canada*
‡ *Department of Radiology & Diagnostic Imaging, University of Alberta, Edmonton, Alberta, Canada*
§ *Department of Medical Physics, Cross Cancer Institute, University of Alberta, Edmonton, Alberta, Canada*
|| *Department of Rheumatology, University of Alberta, Edmonton, Alberta, Canada*
¶ *Department of Oncology, University of Alberta, Edmonton, Alberta, Canada*
# *Department of Physics, University of Alberta, Edmonton, Alberta, Canada*
†† *Department of Biomedical Engineering, University of Alberta, Edmonton, Alberta, Canada*

ARTICLE INFO

Article history:
Received 6 February 2014
Accepted 13 June 2014

Keywords:
Osteoarthritis
MRI
CT
Celecoxib
Glucosamine
Osteophytes

SUMMARY

Objective: We sought to develop a comprehensive scoring system for evaluation of pre-clinical models of osteoarthritis (OA) progression, and use this to evaluate two different classes of drugs for management of OA.

Methods: Post-traumatic OA (PTOA) was surgically induced in skeletally mature rats. Rats were randomly divided in three groups receiving either glucosamine (high dose of 192 mg/kg) or celecoxib (clinical dose) or no treatment. Disease progression was monitored utilizing micro-magnetic resonance imaging (MRI), micro-computed tomography (CT) and histology. Pertinent features such as osteophytes, subchondral sclerosis, joint effusion, bone marrow lesion (BML), cysts, loose bodies and cartilage abnormalities were included in designing a sensitive multi-modality based scoring system, termed the rat arthritis knee scoring system (RAKSS).

Results: Overall, an inter-observer correlation coefficient (ICC) of greater than 0.750 was achieved for each scored feature. None of the treatments prevented cartilage loss, synovitis, joint effusion, or sclerosis. However, celecoxib significantly reduced osteophyte development compared to placebo. Although signs of inflammation such as synovitis and joint effusion were readily identified at 4 weeks post-operation, we did not detect any BML.

Conclusion: We report the development of a sensitive and reliable multi-modality scoring system, the RAKSS, for evaluation of OA severity in pre-clinical animal models. Using this scoring system, we found that celecoxib prevented enlargement of osteophytes in this animal model of PTOA, and thus it may be useful in preventing OA progression. However, it did not show any chondroprotective effect using the recommended dose. In contrast, high dose glucosamine had no measurable effects.

Introduction

Osteoarthritis (OA) is classically characterized by cartilage degeneration, and abnormal bone adaptations such as formation of permanent osteophytes and subchondral bone sclerosis. Despite a number of available palliative treatments, there is currently no disease-modifying treatment. Having a safe pharmacodynamic profile, glucosamine, an amino monosaccharide used in biosynthesis of glycosaminoglycans in articular cartilage, alone or in combination with chondroitin sulfate has been used worldwide for

* Corresponding author. Faculty of Pharmacy & Pharmaceutical Science, 2020J Katz Group-Rexall Centre for Pharmacy & Health Research, University of Alberta, Edmonton, Alberta T6G 2N8, Canada. Tel: 1-780-492-8758.
** Corresponding author. Department of Radiology & Diagnostic Imaging 2A2.41 WMC, University of Alberta Hospital 8440 112 Avenue NW Edmonton, Alberta T6G 2B7, Canada, Tel: 1-780-407-6907.
E-mail addresses: a.panahifar@ualberta.ca (A. Panahifar), jjaremko@ualberta.ca, jjaremko@ualberta.ca (J.L. Jaremko), Anthony.tessier@albertahealthservices.ca (A.G. Tessier), rlambert@ualberta.ca (R.G. Lambert), walter.maksymowych@ualberta.ca (W.P. Maksymowych), bfallone@ualberta.ca (B.G. Fallone), mdoschak@ualberta.ca (M.R. Doschak).

http://dx.doi.org/10.1016/j.joca.2014.06.013
1063-4584/

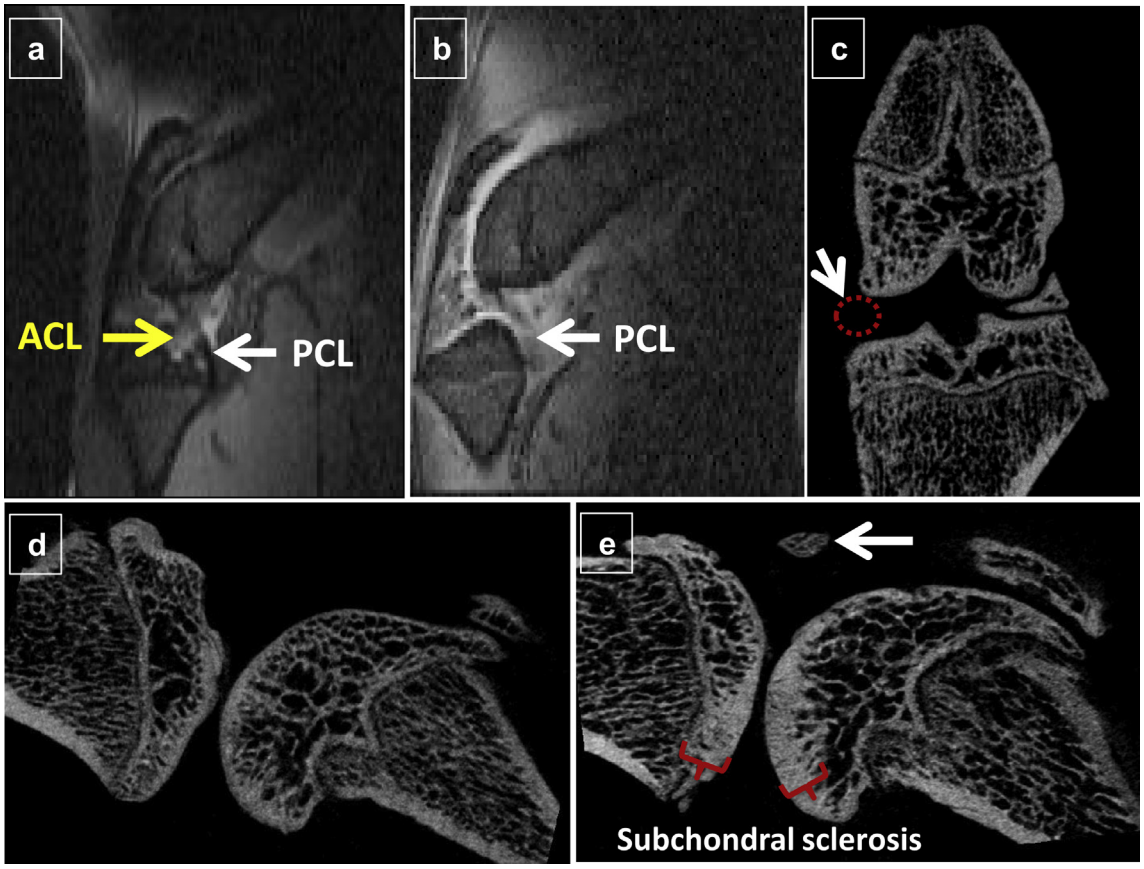

Fig. 1. a) Sagittal T1-weighted/fat suppressed MRI prior to surgery, displaying intact ACL and PCL; b) Sagittal image of the same joint after 12 weeks showing only PCL after transection of ACL (Gd-enhanced); c) coronal micro-CT from the same rat showing absence of medial meniscus (arrow and circle) at 1 day post-surgery. Note that unlike in humans, menisci are ossified in rats. d, e) Sagittal micro-CT of the same joint at baseline (d) and 12 weeks post-surgery (e). Note subchondral sclerosis in femur and tibia (brackets). Also, presence of a mineralized loose body (arrow) that was absent at baseline is notable.

management of OA symptoms, albeit without consensus regarding its disease-modifying capacity[1,2]. Differences in formulation and bioavailability, stage of the disease[2] in experimental groups, and different administered doses[3] have been suggested as factors responsible for the controversy. Furthermore, performing studies in different experimental models as well as variability in outcome measures used makes direct comparisons among these studies challenging.

In the current study we aimed to evaluate the effect of glucosamine and another agent thought to have disease-modifying properties, celecoxib, head-to-head in an established animal model of post-traumatic OA (PTOA). As a prerequisite, it is vitally important to measure the effects of experimented therapeutics using standardized and validated methods for outcome assessment. Several scoring systems exist based on a single modality for use in humans such as the traditional and widely used radiological Kellgren–Lawrence[4] system or newer magnetic resonance imaging (MRI)-based systems like WORMS [5] or BLOKS[6]. However, due to the complex nature of the disease, the measuring system must be not only sufficiently discriminatory to detect minor and early changes, but also assess multiple outcome domains relevant to the clinical and pathophysiological aspects of disease. There are some features that either cannot be detected with one modality or the sensitivity would be low. For instance, we have observed that osteophytes are detectable by computed tomography (CT) long before they appear on MRI or planar X-ray, owing to higher resolution and greater bone/soft tissue contrast of CT (observation from a pilot study, data not shown). Therefore, in the current report we have focused effort towards incorporating as many outcomes as possible to design a comprehensive scoring system.

In this manuscript we describe a comprehensive multimodal approach to the assessment of experimental OA. Bony adaptations such as osteophyte formation, subchondral sclerosis, and the occasional presence of calcified loose bodies were scored mainly by the use of micro-CT. Soft tissue abnormalities including synovitis, joint effusion, cysts, loose bodies and edema were identified and scored using micro-MRI. Cartilage structure at different time points was assessed by histology, as the most sensitive tool for the purpose.

Since animal studies are a prerequisite to human trials, our objective was to develop a multi-modality scoring system combining MRI, CT and histology features applicable to rats as the most available and extensively studied experimental model of OA. However, this system can be easily optimized for use in other animal models. Using this system, we sought to determine whether two controversial therapies, celecoxib and glucosamine, were actually disease-modifying agents in a pre-clinical rat model of PTOA.

Methods and materials

Surgical model of PTOA

PTOA was surgically induced in 27 skeletally mature (9-month-old) Sprague–Dawley rats (Charles River Laboratories, US) by Knee Triad Injury (KTI) surgery[7], with an additional three rats included as

sham-operated control. Briefly, rats were anesthetized with 2% isoflurane, the right knee was shaved and disinfected for operation. A minor incision (1 cm) was made on the medial parapatellar side and the joint capsule was exposed, followed by transection of the medial collateral ligament (MCL). The anterior cruciate ligament (ACL) was carefully transected with micro spring-scissors and the medial meniscus was resected [Fig. 1]. Finally, the joint capsule was flushed with sterile saline and both incisions to the capsule and skin were sutured separately. For sham surgery, the skin was exposed and a similarly sized incision was made to the synovial membrane and sutured without any injury to the MCL, ACL or meniscus. After the surgery all animals received a single subcutaneous dose of meloxicam analgesic (0.1 mg/kg) (Metacam, Boehringer Ingelheim Ltd., CA, USA) and were regularly monitored for signs of discomfort. All animal procedures were carried out in full compliance with the standards of the animal care and use committee of the University of Alberta [see Fig. 2].

Experimental design

KTI-operated animals ($n = 27$) were randomly divided in three groups ($n = 9$ each). The first group received no treatment. The second group received a daily oral dose of celecoxib (Celebrex, Pfizer, USA) using a curved feeding needle at 2.86 mg/kg (calculated based on recommended human dose of 200 mg/day). The third cohort received a daily oral dose of glucosamine hydrochloride (Sigma, USA) at 192 mg/kg (160 mg/kg free base). Three rats from each group were euthanized every 4 weeks for histological analysis. The sham-operated group ($n = 3$) was euthanized at week 12 and did not receive any therapy.

In vivo micro-CT

In vivo micro-CT scans were acquired at 18 μm resolution utilizing Skyscan 1076 (SkyScan NV, Kontich, Belgium). Scans were performed at 1 day post-surgery to confirm complete removal of the meniscus and follow-up was conducted at 4, 8, and 12 weeks. The imaging parameters were set at: voltage = 70 KV, current = 142 μA, exposure time = 1,475 ms, rotation step = 0.5°. Scan time was approximately 42 min. A 1 mm aluminum filter was used to remove low energy X-rays. Projections were reconstructed using a modified Feldkamp back-projection algorithm to obtain cross-sections.

In vivo micro-MRI

In vivo MRI was performed sequentially at 1 day before surgery and 4, 8 and 12 weeks after surgery, utilizing a 9.4 T micro-MRI scanner (Magnex Scientific, Oxford, UK) and a custom-built transmit/receive 25 mm single turn radiofrequency surface coil. Sagittal fat-suppressed T1-weighted (TR 1,250 ms/TE 13 ms) and T2-weighted (TR 3,000 ms/TE 35 ms) spin echo (SE) sequences were acquired at each time point, along with T2-weighted axial images. Field of view was 35 × 20 mm, slice thickness: 0.5 mm, inter-slice gap: 0.1 mm. In addition, contrast-enhanced sagittal and coronal T1-weighted images were acquired at the end-points after Gadolinium (Gd) injection (0.3 mL/kg = 0.15 mmol/kg) as additional method of detecting BMLs.

Histology

After euthanization, right hind limbs were dissected free of soft tissues and fixed in Zamboni's fixative for 10 days, decalcified in Cal-Ex II® (Fisher Scientific, USA) for 4 weeks and the femoral epiphysis sectioned transversely through the origins of the collateral ligaments. 5 μm sections were obtained and stained with Safranin-O/Fast green and H&E.

Scoring system

A multimodality scoring system for application in pre-clinical animal studies was developed in an iterative consensus-building process. This rat arthritis knee scoring system (RAKSS) was tested for sensitivity to change and reliability. The system measures severity of seven primary features of OA: osteophytes, subchondral sclerosis, synovitis-effusion, bony cysts, bone marrow lesions

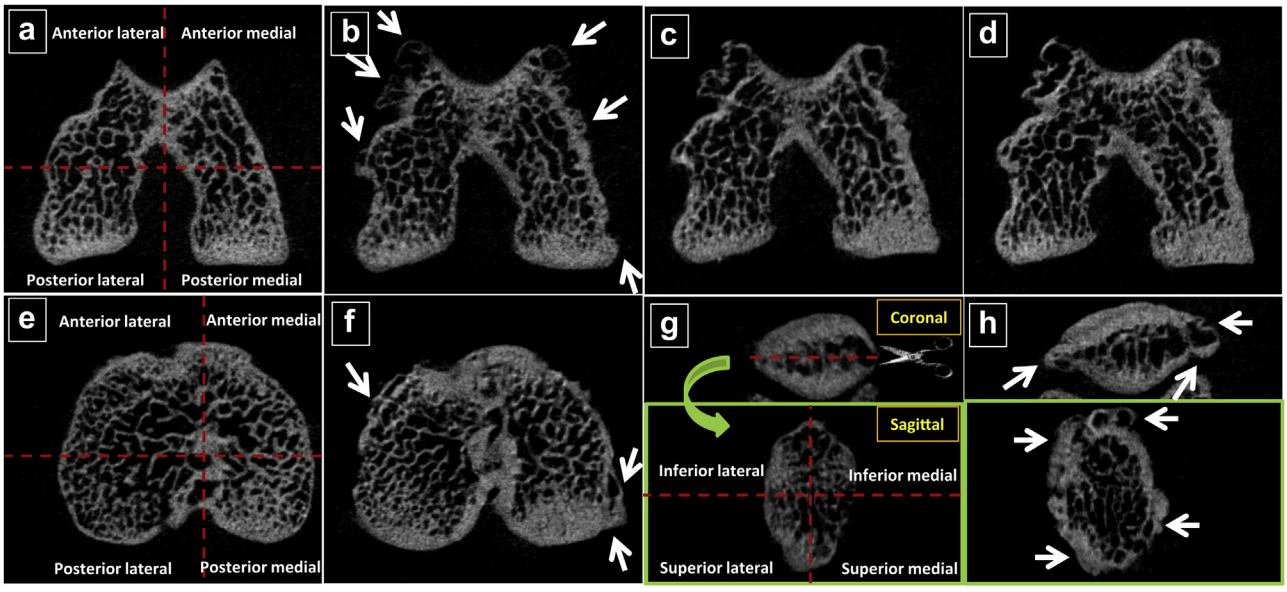

Fig. 2. Micro-CT cross sections showing formation and mineralization of osteophytes at joint margins over time. a) Femur at baseline. The regions used for scoring are illustrated. b–d) The same bone at 4, 8, and 12 weeks post-surgery, respectively. Note the formation of osteophytes around the MCL attachment, trochlear groove, and less pronounced at LCL insertion (arrows). Also, subchondral sclerosis and thickening of bone cortex at medial side are notable. e and f) The images show the transverse view of tibia from the same joint at baseline and 12 weeks post-surgery. g and h) micro-CT images of patella from the same joint at baseline and 12 weeks. Examples of scoring are provided in the Supporting File.

Table I
RAKSS scoring system

Feature	Grade	Modality	Plane
Osteophyte. Femur, tibia, and patella each scored separately at four locations (Fig. 2). Femur and tibia: anterior and posterior medial/lateral, patella: superior and inferior medial/lateral. For each location the maximum score is 2	[0–24]	CT	Femur and tibia: axial Patella: coronal
• None/Possible (maximum depth of osteophyte to bone ≤ 0.2 mm)	0		
• Definite (0.2 mm < ≤0.5 mm)	1		
• Large (>0.5 mm)	2		
Subchondral sclerosis. Femur and tibia scored separately at two locations (medial and lateral). For each location maximum score is 3	[0–12]	CT	Sagittal
• Maximum depth of subchondral plate ≤ 0.3 mm	0		
• 0.3 mm< ≤0.65 mm	1		
• 0.65 mm< ≤1 mm	2		
• >1 mm	3		
Synovitis–effusion. If sum of bright signal at suprapatellar and posterior condyle at both medial and lateral side (4 locations) is:	[0–5]	MRI (T2-weighted)	Axial: Suprapatellar
• ≤ 0.4 mm	0		Sagittal: posterior condyle
• 0.4 mm < ≤1 mm	1		
• 1 mm < ≤2 mm	2		
• 2 mm < ≤3 mm	3		
• 3 mm < ≤4 mm	4		
• >4 mm	5		
Bone cysts. Femur, tibia, and patella scored separately	[0–3]	MRI or CT	Axial/Sagittal
• None	0		
• Present	1		
Loose bodies	[0–3]	MRI or CT	Axial/Sagittal
• None	0		
• Number of bodies = 1	1		
• Number of bodies = 2	2		
• Number of bodies = 3 or more	3		
BML. Femur, tibia, and patella scored separately.	[0–3]	MRI (T2-weighted fat suppressed)	Axial/Sagittal
• None	0		
• Present	1		
Cartilage (directly adopted from modified Mankin's scoring system*)	[0–14]	Histology (H&E and Safranin-O stains)	Transverse
I. Structure			
• Normal	0		
• Surface irregularities	1		
• Pannus and surface irregularities	2		
• Clefts to transitional zone	3		
• Clefts to radial zone	4		
• Clefts to calcified zone	5		
• Complete disorganization	6		
II. Cells			
• Normal	0		
• Diffuse hypercellularity	1		
• Cloning	2		
• Hypocellularity	3		
III. Safranin-O staining			
• Normal	0		
• Slight reduction	1		
• Moderate reduction	2		
• Severe reduction	3		
• No dye noted	4		
IV. Tidemark integrity			
• Intact	0		
• Crossed by blood vessels	1		

(BML), loose bodies and cartilage degeneration. Scoring instructions are given in Table I and examples are provided throughout the article as well as in a Supporting File.

All CT datasets were rotated to the transverse plane (relative to the tibia) and stored at sagittal, axial, and coronal planes for later use. Osteophytes were scored separately for femur, tibia and patella at four regions. The maximum depth of osteophyte perpendicular to bone was measured and scored in a two scale score (maximum of eight for each bone). Depth of less than 0.2 mm was considered ambiguous and scored 0. The reference plane for scoring femur and tibia was axial and for the patella, coronal. Osteophytes were scored based on CT, although large osteophytes were visible on MRI.

Subchondral sclerosis was evaluated in the femur and tibia at both medial and lateral sides based on a three scale score (a maximum score of six for each bone). Sclerosis was defined as a solid mineralized region with no distinct trabecular structure. The depth of sclerosis was measured on sagittal CT, from the articular surface along the diaphysis and the maximum value was reported. Baseline data were analyzed and depth of up to 0.3 mm was considered normal thickness of subchondral bone plate.

Synovitis and joint effusion were scored together (Table I), and measured as the sum of maximum length of bright signal perpendicular to bone on T2 fat-suppressed MRI, at four locations eminent for presence of synovitis-effusion; suprapatellar and posterior to both condyles. The severity was graded based on the

Table II
Mean scores and comparisons

Feature	Baseline ($n = 3$)	4 Weeks ($n = 3$)	8 Weeks ($n = 3$)	12 Weeks ($n = 3$)	Baseline ($n = 3$)	4 Weeks $n = 3$)	8 Weeks ($n = 3$)	12 Weeks ($n = 3$)
	Untreated				***Sham-operated control***			
Femur osteophyte	†0	5, [2.52, 7.48]	5.6, [4.23, 7.10]	7, [4.52, 9.48]	†0	†0 $P < 0.001$	†0 $P < 0.001$	†0 $P < 0.001$
Tibia osteophyte	†0	4.6, [1.80, 7.54]	5.3, [2.46, 8.20]	4.3, [2.90, 5.77]	†0	†0 $P = 0.002$	†0 $P < 0.001$	†0 $P < 0.001$
Patella osteophyte	†0	3.6, [−6.37, 13.71]	4.6, [−2.50, 11.84]	6, [1.70, 10.30]	†0	†0 $P = 0.008$	†0 $P = 0.049$	†0 $P = 0.004$
Osteophyte total	†0	13.3, [3.93, 22.74]	15.6, [5.63, 25.71]	17.3, [10.16, 24.50]	†0	†0 $P = 0.004$	†0 $P = 0.003$	†0 $P < 0.001$
Sclerosis medial femur	0.3, [−1.10, 1.77]	†2	2.3, [0.90, 3.77]	2.3, [0.90, 3.77]	0.5, [−0.85, 1.15]	†0.5, [−0.85, 1.15], $P = 0.028$	†0.5, [−0.85, 1.15], $P = 0.049$	†0 $P = 0.012$
Sclerosis lateral femur	†0	†0	†0	†0	†0	†0	†0	†0
Sclerosis medial tibia	†0	1.3, [−0.10, 2.77]	†2	†2	†0	†0 $P = 0.05$	†0.5, [−0.85, 1.15], $P = 0.028$	†0 $P = 0.046$
Sclerosis lateral tibia	†0	†0	†0	†0	†0	†0	†0	†0
Synovitis-effusion total	†0	3.6, [2.23, 5.10]	3.6, [2.23, 5.10]	3.3, [1.90, 4.77]	†0	1.5, [−0.85, 1.15], $P = 0.032$	0.5, [−0.85, 1.15], $P = 0.011$	1.5, [−0.85, 2.85], $P = 0.049$
Bone cysts total	0.3, [−1.10, 1.77]	0.3, [−1.10, 1.77]	0.6, [−0.77, 2.10]	†1	1, [1.71, 3.71], $P = 0.495$	1, [1.71, 3.71], $P = 0.495$	1, [−1.71, 3.71], $P = 0.724$	1, [−1.71, 3.71], $P = 1.00$
BML total	†0	0.3, [−1.10, 1.77]	0.3, [−1.10, 1.77]	0.3, [−1.10, 1.77]	†0	†0 $P = 0.495$	†0 $P = 0.495$	†0 $P = 0.495$
Loose bodies	†0	0.6, [−0.77, 2.10]	1, [−1.48, 3.48]	0.6, [−2.20, 3.54]	†0 $P = 0.219$	†0 $P = 0.219$	†0 $P = 0.272$	†0 $P = 0.495$
Cartilage structure	N/A	5.3, [3.90, 6.77]	5.3, [2.46, 8.20]	†6	N/A	†0 $P < 0.001$	N/A	†0 $P < 0.001$
Cartilage cells	N/A	2.3, [0.90, 3.77]	2.3, [−0.54, 5.20]	†3	N/A	†0 $P < 0.001$	N/A	†0 $P < 0.001$
Cartilage Safranin-O staining	N/A	†1	1.3, [−0.10, 2.77]	1.3, [−0.10, 2.77]	N/A	†0 $P = 0.009$	N/A	†0 $P = 0.009$
* Cartilage tidemark integrity	N/A	†0	†0	†0	N/A	†0	N/A	†0
Cartilage total	N/A	8.6, [5.80, 11.54]	9, [4.70, 13.30]	10.3, [8.90, 11.77]	N/A	0 $P < 0.001$	N/A	0 $P < 0.001$
	Celecoxib				***Glucosamine***			
Femur osteophyte	†0	1.6, [0.23, 3.10], $P = 0.007$ $\mathbf{P < 0.001}$	3.3, [1.90, 4.77], $P = 0.008$ $\mathbf{P = 0.016}$	4, [1.52, 6.48], $P = 0.021$ $\mathbf{P = 0.028}$	†0	5.6, [4.23, 7.10], $P = 0.374$	6.3, [3.46, 9.20], $P = 0.422$	†7 $P = 1.00$
Tibia osteophyte	†0	1, [−1.48, 3.48], $P = 0.014$ $\mathbf{P = 0.07}$	2.6, [−1.13, 6.46], $P = 0.073$ $\mathbf{P = 0.519}$	2.3, [−0.54, 5.20], $P = 0.055$ $\mathbf{P = 0.148}$	†0	3, [0.52, 5.48], $P = 0.132$	3.3, [1.90, 4.77], $P = 0.055$	†4 $P = 0.495$
Patella osteophyte	†0	1.3, [−0.10, 2.77], $P = 0.378$ $\mathbf{P = 0.004}$	2.3, [−1.46, 6.13], $P = 0.284$ $\mathbf{P = 0.32}$	2.6, [−0.20, 5.54], $P = 0.05$ $\mathbf{P = 0.138}$	†0	4, [−0.97, 8.97], $P = 0.904$	4.6, [−3.32, 12.65], $P = 1.00$	5.5, [−1.56, 15.56], $P = 0.789$
Osteophyte total	†0	4, [−0.97, 8.97], $P = 0.02$ $\mathbf{P = 0.015}$	8.3, [0.74, 15.92], $P = 0.066$ $\mathbf{P = 0.139}$	9, [4.70, 13.30], $P = 0.013$ $\mathbf{P = 0.022}$	†0	12.6, [5.08, 20.26], $P = 0.824$	14.3, [2.59, 26.07], $P = 0.729$	16.5, [1.27, 25.56], $P = 0.754$
Sclerosis medial femur	0.3 [−1.10, 1.77]	†1 $P = 0.025$ $\mathbf{P = 0.025}$	†2 $P = 0.43$ $\mathbf{P = 1.00}$	†2 $P = 0.374$ $\mathbf{P = 1.00}$	†0	†2 $P = 1.00$	†2 $P = 0.374$	†2 $P = 0.495$
Sclerosis lateral femur	†0	†0	†0	†0	†0	†0	†0	†0
Sclerosis medial tibia	†0	1.3, [−0.1, 2.77], $P = 1.00$ $\mathbf{P = 0.114}$	†2 $P = 1.00$ $\mathbf{P = 1.00}$	†2 $P = 1.00$ $\mathbf{P = 1.00}$	†0	†2 $P = 0.116$	†2 $P = 1.00$	†2 $P = 1.00$
Sclerosis lateral tibia	†0	†0	†0	†0	†0	†0	†0	†0

(*continued on next page*)

Table II (*continued*)

Feature	Baseline ($n = 3$)	4 Weeks ($n = 3$)	8 Weeks ($n = 3$)	12 Weeks ($n = 3$)	Baseline ($n = 3$)	4 Weeks $n = 3$)	8 Weeks ($n = 3$)	12 Weeks ($n = 3$)
Synovitis−effusion total	†0	3.6, [2.23, 5.10], $P = 1.00$ **$P = 0.317$**	†3 $P = 0.116$ **$P = 0.025$**	3.3, [1.90, 4.77], $P = 1.00$ **$P = 0.789$**	†0	†4 $P = 0.374$	†4 $P = 0.374$	3.5 [0.85, 7.85], $P = 0.789$
Bone cysts total	†0	0.6, [−0.77, 2.10], $P = 0.519$ **$P = 1.00$**	1, [−1.48, 3.48], $P = 0.643$ **$P = 1.00$**	1.6, [0.23, 3.10], $P = 0.116$ **$P = 0.495$**	0.3, [−1.10, 1.77], $P = 0.519$	0.6, [−0.77, 2.10], $P = 0.519$	0.6, [−0.77, 2.10], $P = 0.643$	1, −6.71, 6.71], $P = 1.00$
BML total	†0	†0, $P = 0.374$ **$P = 1.00$**	†0, $P = 0.374$ **$P = 1.00$**	†0, $P = 0.374$ **$P = 1.00$**	†0	†0 $P = 0.495$	†0 $P = 0.495$	†0 $P = 0.495$
Loose bodies	†0	0.3, [−1.10, 1.77], $P = 0.519$ **$P = 0.519$**	0.6, [−0.77, 2.10], $P = 0.643$ **$P = 1.00$**	1, [−1.48, 3.48], $P = 0.725$ **$P = 1.00$**	†0	0.6, [−0.77, 2.10], $P = 1.00$	0.6, [−0.77, 2.10], $P = 0.643$	†1 $P = 0.724$
Cartilage structure	N/A	5, [2.52, 7.48], $P = 0.643$ **$P = 0.374$**	†6 $P = 0.374$ **$P = 1.00$**	†6 $P = 1.00$ **$P = 1.00$**	N/A	5.6, [4.23, 7.10], $P = 0.519$	†6 $P = 0.495$	†6 $P = 1.00$
Cartilage cells	N/A	1.6, [−2.13, 5.46], $P = 0.519$ **$P = 0.205$**	2.6, [1.23, 4.10], $P = 0.674$ **$P = 0.495$**	†3 $P = 1.00$ **$P = 0.272$**	N/A	†3 $P = 0.116$	†3 $P = 0.495$	†3 $P = 1.00$
Cartilage Safranin-O staining	N/A	1.3, [−0.1, 2.77], $P = 0.374$ **$P = 0.422$**	1, [−0.77, 2.10], $P = 0.230$ **$P = 0.789$**	†1 $P = 0.374$ **$P = 0.221$**	N/A	0.6, [−2.20, 3.54], $P = 0.643$	0.5, [−0.10, 2.77], $P = 0.239$	1.5, [−0.10, 2.77], $P = 0.789$
*Cartilage tidemark integrity	N/A	†0	†0	†0	N/A	†0	†0	†0
Cartilage total	N/A	8, [3.70, 12.30], $P = 0.609$ **$P = 0.374$**	**$P = 0.870$**	†10 $P = 0.374$ **$P = 0.272$**	N/A	9.3, [5.54, 13.13], $P = 0.579$	9.5, [8.23, 11.10], $P = 0.735$	10.5, [8.90, 11.77], $P = 0.789$

The table represents the mean scores for each cohort. 95% confidence intervals are reported in brackets for each estimate.

* No statistics available because all observational values were zero.

† No confidence interval available because all observational values were the same. Comparisons between untreated and treatment groups, and between untreated and sham-operated groups, were performed by two-way independent *t*-test at each respective time-point. Comparison between celecoxib and glucosamine were performed and indicated by **bold *P*-values**. Non-parametric Mann−Whitney *U*-test was substituted if standard deviation was zero (i.e., sclerosis scores). In glucosamine group severity of no feature was statistically different from untreated group.

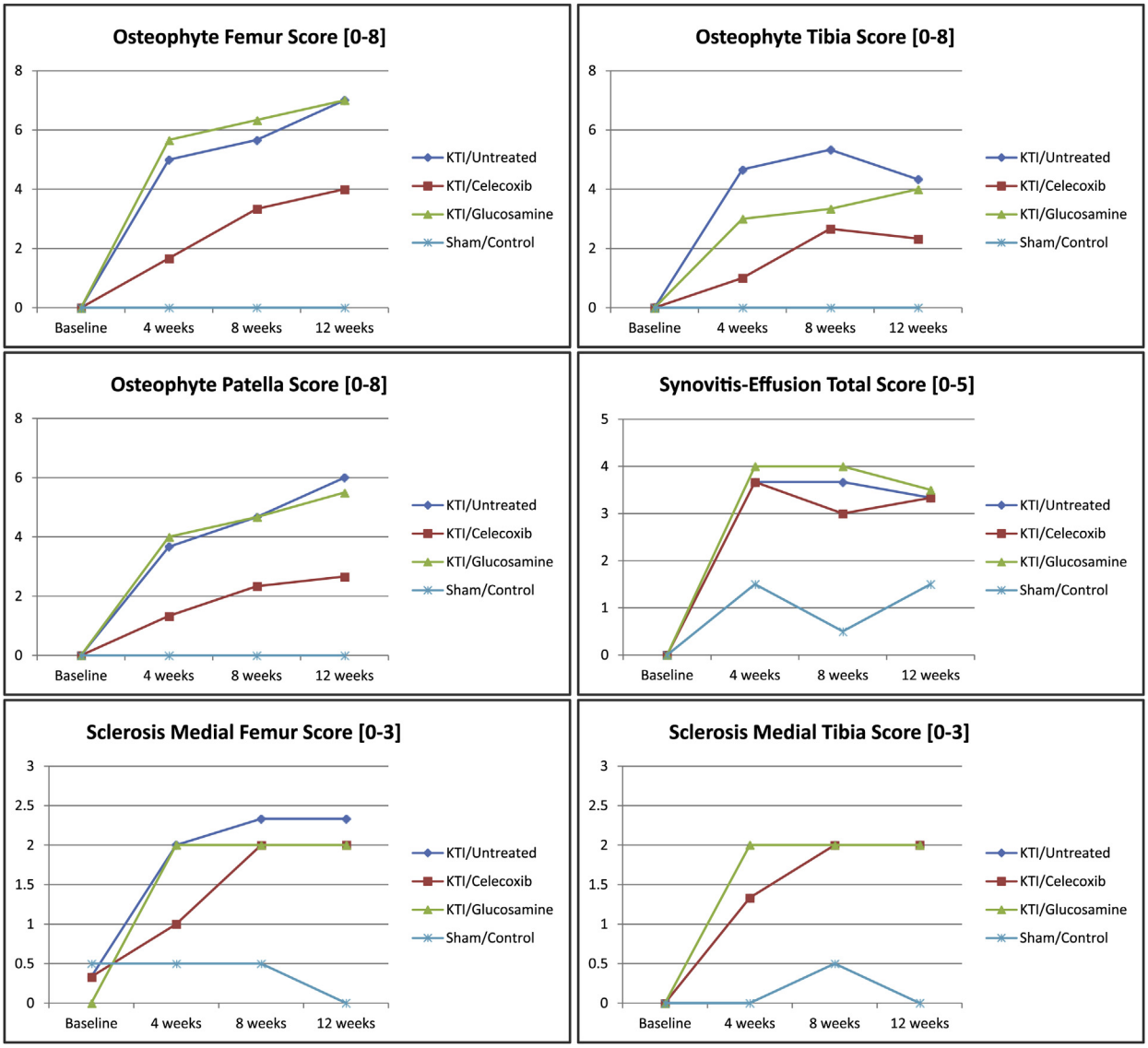

Fig. 3. Graphs represent the changes of mean scores over time for each treatment cohort. Number of observation at each time-point was $n = 3$. See Table II for detailed mean scores and comparisons.

combined length of signal for each joint, in afive scale grading system.

Because cysts in this model were mainly bony cysts, only bony cysts were graded. Cysts were clearly visible on both CT and MRI and were defined as round structures with no trabeculae, recognizable from hyper-intense signal on T2 fat-suppressed MRI or black structures (i.e., lack of minerals) on CT. The assessment was performed for all three bones, primarily on sagittal plane in a dichotomous grade; absent = 0, present = 1.

Loose bodies were graded based on their number present in the synovial capsule where; 0 = none, 1 = 1 loose body; 2 = 2 loose bodies; 3 = 3 or more. The presence of bodies was confirmed after assessment with axial and sagittal MRI images.

Because of the small size of knee joint in rats, a simple binary system similar to HIMRISS[8] was adopted for grading BMLs. In each bone, a score of 1 is awarded if there is a BML on T2 fat-suppressed SE MRI. Additional Gd-enhanced T1 sequences were acquired at the final time-point.

Modified Mankin's scoring system for OA[9,10] was adapted to evaluate cartilage integrity on H&E and Safranin-O/Fast green stained histology sections.

To assess inter-observer reliability, two readers blinded to the treatment cohorts independently reviewed subsets of data at 4 and 12 weeks: a doctoral student trained in CT and MR imaging (AP), and a board certified, fellowship trained musculoskeletal radiologist (JJ).

Statistical analysis

Statistical analysis was conducted using SPSS software, version 17.0. For group comparisons, two-tailed independent *t*-test was used ($P < 0.05$). If standard deviations were zero and *t*-test was not feasible, two-tailed Mann–Whitney *U*-test was substituted ($P < 0.05$). Reliability was assessed by intra-class correlation coefficient or percent agreement for status of each OA feature. In addition, synovitis–effusion and subchondral sclerosis were

Table III
Reliability of the scoring system measured by inter-observer correlation coefficient (ICC) (status of features)

Feature	ICC	*N*
Femur osteophyte score	0.756	24
Tibia osteophyte score	0.854	24
Patella osteophyte score	0.849	24
Total osteophyte score	0.853	24
Synovitis–Effusion total score	0.867	43
Femur cyst score	0.790	22
Tibia cyst score	0.647	22
Patella cyst score	N/A*	22
Total cyst score	0.819	22
BML total score	N/A*	43

* Frequency of BML was too low to accurately calculate ICC, thus % agreement was measured and reported as 93.02. Also, no patellar cyst was observed.

Table IV
Correlation of semi-quantitatively measured scores based on RAKSS with absolute quantified values measured by micro-CT or micro-MRI

Feature	*R*	Significance	*n*
Total osteophyte	+0.801	0.05	6
Synovitis–Effusion	+0.984	0.01	43
Sclerosis medial femur	+0.951	0.01	43
Sclerosis medial tibia	+0.965	0.01	43

A two-tailed Pearson correlation for the data revealed that scores for osteophytes, synovitis-effusion and sclerosis were significantly correlated with the absolute values. Therefore, designed system is representative of the actual values of these features.

quantified by measuring the length of the occurring feature and correlation with their respective scores were assessed by Pearson's correlation. Also, a randomly selected subset of samples ($n = 6$) were quantified for volumetric size of osteophytes (% BV/TV) and correlated with scores. Only a subset was included because this sample size was sufficient for the purpose of showing the correlation between absolute and semi-quantitative scores, and also the procedure is laborious and time-consuming.

Results

Generally, in this animal model, most of the changes occurred in the medial compartment where surgery was performed. The most evident characteristics were rapid formation of osteophytes within 4 weeks post-surgery, primarily proximal to the MCL and LCL insertions and the margins of the patellofemoral articulating surfaces. The majorities of osteophytes were developed by week 4 and were only mineralized further by elapsing time. Celecoxib treatment significantly reduced enlargement of osteophytes at 4 weeks ($P < 0.01$) and 12 weeks ($P < 0.05$). While significant reduction was also witnessed at the 8th week for the femur ($P < 0.05$), tibia, patella, and total scores were not statistically lower. The mean scores and comparison between treated and untreated cohorts, as well as direct comparison between celecoxib and glucosamine are reported in Table II. Fig. 3 shows changes of selected features over time.

ICC for status of the analyzed features was generally greater than 0.750 which shows good agreement between observers (Table III). Good inter-observer agreements show that each feature can be reliably measured based on the criteria of the RAKSS. Furthermore, significant differences between sham-operated and untreated KTI-operated cohorts (Table II), revealed that this system is sensitive to the changes following surgery and OA progression, regardless of the type of treatment.

As previously mentioned, continuously progressing features were quantified for all or a subset of dataset. Table IV represents significant correlation between absolute quantified measures and semi-quantitative scores for osteophytes, synovitis-effusion, and subchondral sclerosis. Subchondral sclerosis scores correlated strongly with bone plate thickness for both femur and tibia, with $R = +0.951$ and $+0.965$, respectively ($P < 0.01$). Except at week 4, where sclerosis in the celecoxib group at the medial femoral condyle was significantly lower compared with untreated or glucosamine cohorts, all other time-points did not show any significant difference regarding femoral or tibial sclerosis.

Inflammatory signs were readily visible by week 4 in all KTI-operated animals. Synovitis and effusion were scored collectively, and were not significantly different among groups. The extent of synovitis-effusion was slightly reduced over time in all groups, but not significantly. The greatest measure was observed in the glucosamine group where a score of 4 at weeks 4 and 8 corresponded to a combined length of 3.37 mm and 3.55 mm, respectively.

Bony cysts were present randomly among all treatment groups and treatment did not affect their presence. As the disease progressed, total numbers of cysts increased from 4 to 23 from baseline to week 12 (combining all 27 animals together). The most prominent sites for cysts were posterior medial tibia and femur, accounting for 39% and 17% of cysts at week 12, respectively. Occasionally, a few cysts were observed to resolve over time, but generally cysts persisted until the end-point and new cysts were formed as well.

Loose bodies were absent at baseline, but started to appear at week 4 when 6 bodies were present in a total of 27 rats. This number grew to 10 by week 12. 60% of these bodies were located in the medial compartment of the joint. Some initially cartilaginous bodies became calcified later and eventually visible on CT [Fig. 1(e)].

Except for occasional ill-defined hyper-intense signals on T2-fat suppressed MRI, no BML were observed during the 12 weeks monitoring of animals. However, careful examination of the histological sections revealed histopathological characteristics of BML such as bone marrow edema or fibrosis [Fig. 4(K), (L)].

Severe cartilage destruction was observed in KTI-operated animals, likely as a result of aberrant excessive loading and joint instability. Glucosamine and celecoxib did not prevent cartilage destruction and almost the entire articular cartilage thickness was degraded by week 4 and calcified cartilage was exposed. By week 8, calcified cartilage was absent, underlying subchondral bone was exposed, and eburnation was visibly noticeable in all samples [Fig. 5]. There was no statistical difference between treatment groups in any studied feature of cartilage pathology (Table II). Sham-operated animals did not reveal any cartilage abnormalities.

Discussion

We evaluated two controversial OA therapies in a rat model of post-traumatic OA. Since current clinical scoring systems for severity assessment of human OA are not directly transferable for use in animal studies (because some features assessed in humans may not be present in animals due to anatomical and biological differences, or may be different based on the method of OA induction), we first needed to develop a reliable multi-modality scoring system. The RAKSS scoring system reported here scores various features relevant to OA progression using MRI and CT. We found it to be sensitive to disease progression over time and changes as a result of treatment. Moreover, the reliability tests showed that changes following OA induction surgery were detected with a high degree of inter-observer agreement.

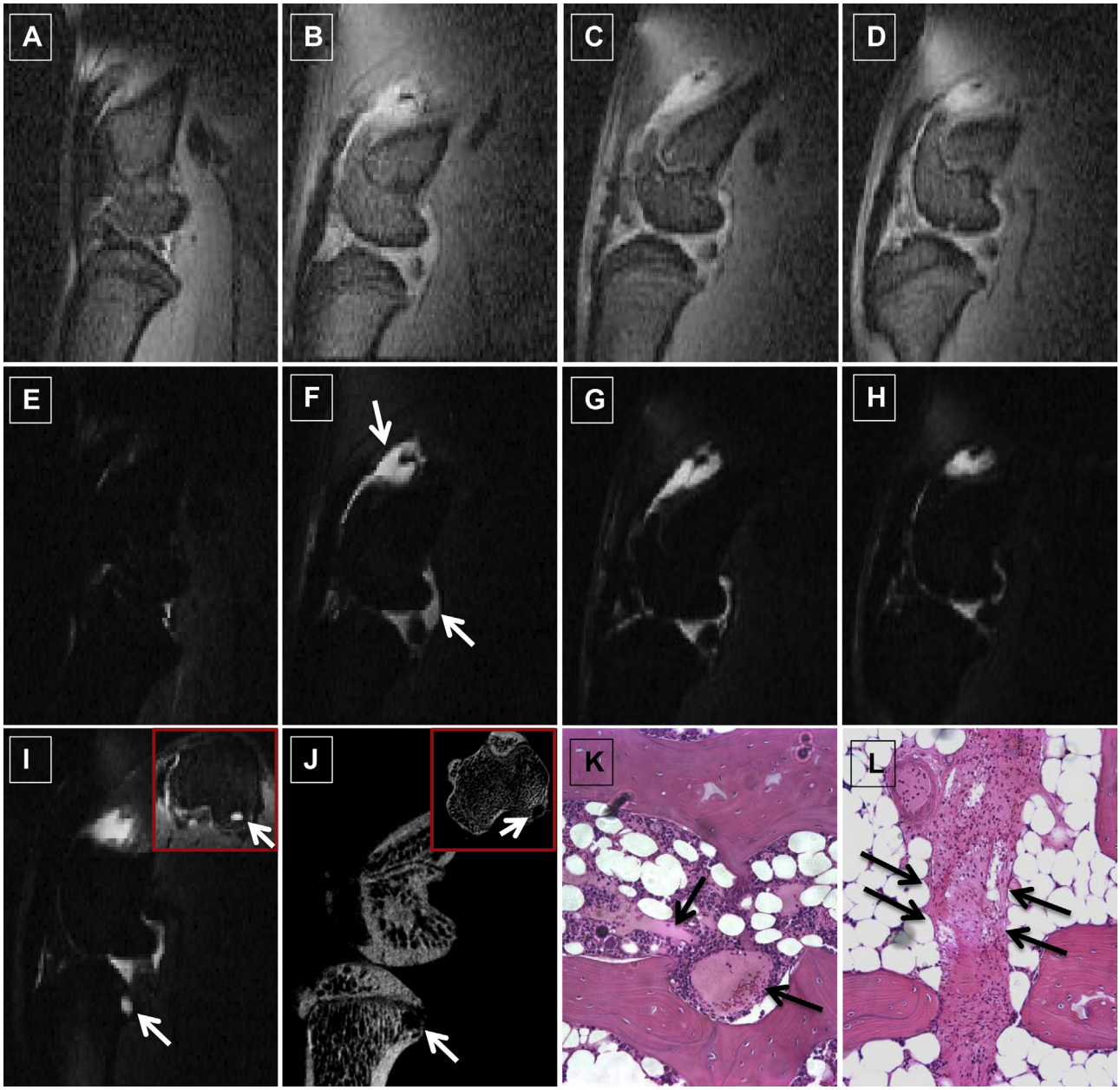

Fig. 4. Temporal MRI from a KTI-untreated rat. A–D) Sagittal T1-weighted fat-saturated MRI before and after surgery at 4, 8, and 12 weeks, respectively. E–F) Sagittal T2 fat-saturated images of the same joint indicating fluctuations in the degree of synovitis-effusion at suprapatellar region and posterior to condyle (arrows). I) Periarticular cyst (arrow) on sagittal T2 fat-saturated MRI and the corresponding micro-CT image (J). Inlets represent axial view. K, L) H&E histology sections of medial femur showing pathological characteristics of BML including bone marrow edema (arrows in K) and bone marrow fibrosis (arrows in L).

Osteophytes in this model were observed bilaterally, but were larger in the medial compartment, with the exception of the patella. Our group has previously investigated osteophyte development in a meniscectomy model[11], where the pattern was different and more pronounced around the MCL and the articulating surfaces of the femur with the tibia. In contrast to a recent report[12], we found that despite similarly altered mechanical loading, animals treated with a COX-2 inhibitor drug (i.e., celecoxib) had significantly smaller osteophytes 4–12 weeks post-injury. The mechanism for this remains unclear, whether due to direct inhibition of COX-2 enzyme, or indirect down-regulation of transforming growth factor-beta 1 (TGF-β1)[13,14], IGF-1[15,16] or other factors involved in osteophytogenesis. Prostaglandin E2 (PGE2), a metabolite of COX-2 known to up-regulate receptor activator of NF-κB ligand (RANKL) may also play a role by stimulating bone resorption at sites of osteophytosis and subsequently leading to further expansion of osteophytes[17]. Further experiments using higher doses of celecoxib may prove to be beneficial.

Cysts were clearly detectable on both CT and MRI; however, CT more accurately detected smaller cysts because of higher spatial resolution. When scoring cysts, attention must be paid not to misinterpret anatomical notches in the femoral condyle and tibia for cysts. Evaluation with multiple planes is therefore strongly recommended. As previously mentioned, cysts were primarily observed in the posterior medial compartments where cartilage was completely destroyed by weeks 4–8. These findings are in agreement with previous findings in humans[5] and may be linked to increased loading in the region due to instability of the joint[18].

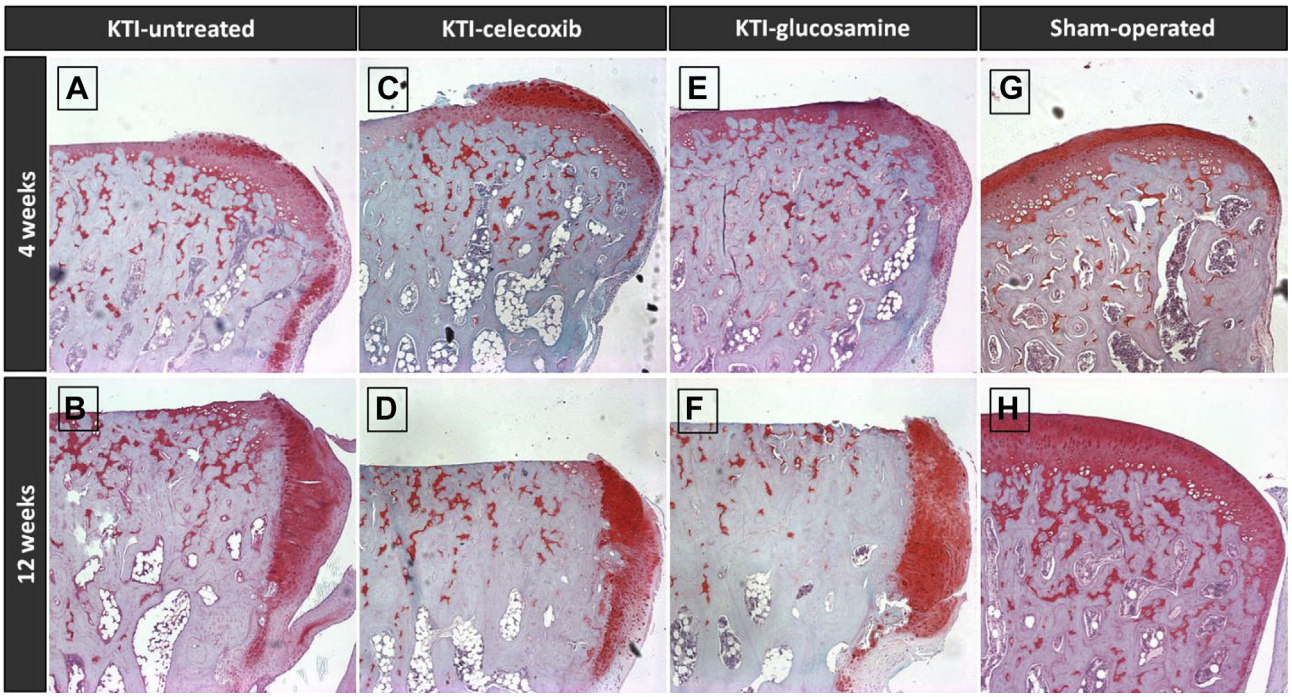

Fig. 5. Histology sections (5×, Safranin-O/Fast green) of femur at transverse plane showing the progression of cartilage loss at 4 and 12 week time-points in animals underwent KTI surgery. A, B) KTI-untreated; C, D) KTI-celecoxib treated group; E, F) KTI-glucosamine treatment; G, H) Sham-operated control group. Approximately the entire articular cartilage thickness had been destroyed by week 4 on KTI-operated rats, regardless of treatment. Note formation of osteophytes at junction of articular cartilage with bone.

In the current study we did not detect any BML in rats on MRI, despite seeing changes in marrow on histology such as bone marrow edema and fibrosis[19,20] [Fig. 4(K), (L)] that are associated with BML on MRI of human joints. BML have been studied in humans extensively in recent years and are associated with progressive OA by various postulated mechanisms[21–23]. Moreover, BMLs have been reported in large animal models[24], but not consistently in small animals. One explanation could be greater susceptibility artifact at high-field MRI that subsequently results in inhomogeneous fat suppression that itself may mask BML signal[25,26]. In this research fat suppression was optimized individually for each rat. However, we did not detect BML signal even after Gd enhancement or on spin-echo T1 images where susceptibility is minimized. Appel *et al.*[27] correlated the histopathology and MRI appearance of BML in ankylosing spondylitis and reported that small areas of histopathological interstitial edema cannot be detected by MRI. Since synovial fluid was adequately visualized on SE/fat suppressed sequences, we speculate that BML were not detected in these rats possibly because of their small size. Partial volume effect in these small ROIs could also be contributory. Future studies investigating BML may consider using larger animal models such as dog or rabbit.

Although we used high resolution micro-MRI, the tiny plates of cartilage in rats were still too thin to be adequately visualized using conventional pulse-sequences, showing volume averaging with synovial joint fluid. This was more pronounced in severe OA cases where most of the cartilage thickness was lost. Cartilage is more sensitively assessed at histology. In this study, none of the treatments had any effect on preserving cartilage thickness.

Historically, OA was characterized as a non-inflammatory disease. However, the presence of inflammatory features, such as synovitis and joint effusion in the current model and other studies, strongly suggest the existence of different sub-types (or phenotypes) of OA, rather than the traditional classification of primary and secondary OA[28,29]. A pathological role for inflammation, specifically for synovium has been suggested[30,31], where secretion of inflammatory cytokines accelerates cartilage erosion and promotes osteophytosis. Therefore, inflammation may be a relevant target for treatment of OA. Massicotte *et al.*[15] demonstrated that prevalence of subchondral sclerosis may be directly related to the levels of Insulin-like growth factor 1 (IGF-1), so that patients may be categorized into groups with a high or low risk of sclerosis. Further research may better explain why patients progress at different rates and to a different degree, have different symptoms, and respond differently to treatment.

The KTI surgical model we used is a very rapidly progressing model for development of OA-like symptoms, since by 4 weeks osteophytes, joint effusion, subchondral sclerosis and extensive cartilage degradation were observed. Symptoms at week 12 already correspond to late stage OA. Depending on study objectives, future studies may choose a shorter end-point for this model or a more subtle injury such as isolated meniscectomy that may produce a milder arthropathy. However, we deliberately chose a late end-point (determined by complete degradation of cartilage) for determining maximal cut-offs in designing the scoring system. The small number of animals in each group was considered as a limitation of the study. This was due to the considerable expenses of micro-MRI and micro-CT imaging; however, the temporal nature of *in vivo* imaging partly compensates for that. A relatively large number of *t*-tests were performed on this small data set, and approximately 5% of these can be expected to give incorrect results. This is unlikely to materially affect the conclusions of the study.

In conclusion, herein we report development of a sensitive and reliable multi-modality scoring system (RAKSS) for evaluation of OA severity in animal models. This scoring system may help to precisely evaluate the efficacy of novel compounds for treatment of OA. Using RAKSS, we conclude that high doses of glucosamine (10 times higher than recommended dose) did not have any effect on preserving cartilage or any other beneficial effect in this animal model of PTOA. On the other hand, celecoxib controlled further

enlargement of osteophytes, but did not show any chondroprotective effect using recommended dose. Although due to small animal numbers, strong conclusions cannot be made and further studies are required, overall we suggest that celecoxib may possess some disease-modifying properties for management of OA.

Author contributions

Conception and design: AP, JJ and MRD. Collection and assembly of data: AP. Analysis and interpretation of the data: AP, JJ and MRD. Statistical expertise: AP and JJ. Obtaining of funding: MRD and WPM. Drafting of the article: AP and MRD. Revising manuscript content: AP, JJ, RGL, WPM and MRD. Final approval of the article: AP, JJ, RGL, WPM, AGT, BGF, and MRD. MRD takes responsibility for the integrity of the data analysis.

Competing interests

The authors have no competing interests or conflicts of interest.

Funding sources

This research was funded by the Canadian Institutes for Health Research (CIHR) and the Osteoarthritis Alberta Team Grant from the Alberta Innovates Health Solutions.

Acknowledgments

The authors would like to thank Dr. Nicola De Zanche for assistance in building and repair of MRI RF coils and Gail Hipperson for catheter placement during Gd experiment.

Supplementary data

Supplementary data related to this article can be found at http://dx.doi.org/10.1016/j.joca.2014.06.013.

References

1. McAlindon TE, LaValley MP, Gulin JP, Felson DT. Glucosamine and chondroitin for treatment of osteoarthritis: a systematic quality assessment and meta-analysis. JAMA 2000 Mar 15;283(11):1469–75.
2. Sawitzke AD, Shi H, Finco MF, Dunlop DD, Bingham 3rd CO, Harris CL, *et al*. The effect of glucosamine and/or chondroitin sulfate on the progression of knee osteoarthritis: a report from the glucosamine/chondroitin arthritis intervention trial. Arthritis Rheum 2008 Oct;58(10):3183–91.
3. Aghazadeh-Habashi A, Jamali F. The glucosamine controversy; a pharmacokinetic issue. J Pharm Pharm Sci 2011;14(2):264–73.
4. Kellgren JH, Lawrence JS. Radiological assessment of osteo-arthrosis. Ann Rheum Dis 1957 Dec;16(4):494–502.
5. Peterfy CG, Guermazi A, Zaim S, Tirman PF, Miaux Y, White D, *et al*. Whole-organ magnetic resonance imaging score (WORMS) of the knee in osteoarthritis. Osteoarthritis Cartilage 2004 Mar;12(3):177–90.
6. Hunter DJ, Lo GH, Gale D, Grainger AJ, Guermazi A, Conaghan PG. The reliability of a new scoring system for knee osteoarthritis MRI and the validity of bone marrow lesion assessment: BLOKS (Boston Leeds Osteoarthritis Knee Score). Ann Rheum Dis 2008 Feb;67(2):206–11.
7. Hayami T, Pickarski M, Wesolowski GA, McLane J, Bone A, Destefano J, *et al*. The role of subchondral bone remodeling in osteoarthritis: reduction of cartilage degeneration and prevention of osteophyte formation by alendronate in the rat anterior cruciate ligament transection model. Arthritis Rheum 2004 Apr;50(4):1193–206.
8. Jaremko JL, Lambert RG, Zubler V, Weber U, Loeuille D, Roemer FW, *et al*. Methodologies for semiquantitative evaluation of hip osteoarthritis by magnetic resonance imaging: approaches based on the whole organ and focused on active lesions. J Rheumatol 2014 Feb;41(2):359–69.
9. Mankin HJ, Dorfman H, Lippiello L, Zarins A. Biochemical and metabolic abnormalities in articular cartilage from osteo-arthritic human hips. II. Correlation of morphology with biochemical and metabolic data. J Bone Jt Surg Am 1971 Apr;53(3):523–37.
10. van der Sluijs JA, Geesink RG, van der Linden AJ, Bulstra SK, Kuyer R, Drukker J. The reliability of the Mankin score for osteoarthritis. J Orthop Res 1992 Jan;10(1):58–61.
11. Panahifar A, Maksymowych WP, Doschak MR. Potential mechanism of alendronate inhibition of osteophyte formation in the rat model of post-traumatic osteoarthritis: evaluation of elemental strontium as a molecular tracer of bone formation. Osteoarthritis Cartilage 2012 Jul;20(7):694–702.
12. Fukai A, Kamekura S, Chikazu D, Nakagawa T, Hirata M, Saito T, *et al*. Lack of a chondroprotective effect of cyclooxygenase 2 inhibition in a surgically induced model of osteoarthritis in mice. Arthritis Rheum 2012 Jan;64(1):198–203.
13. van Beuningen HM, van der Kraan PM, Arntz OJ, van den Berg WB. Transforming growth factor-beta 1 stimulates articular chondrocyte proteoglycan synthesis and induces osteophyte formation in the murine knee joint. Lab Invest 1994 Aug;71(2):279–90.
14. Liu H, Peng Y, Liu F, Li J, Chen X, Liu Y, *et al*. A selective cyclooxygenase-2 inhibitor decreases transforming growth factor-beta1 synthesis and matrix production in human peritoneal mesothelial cells. Cell Biol Int 2007 May;31(5):508–15.
15. Massicotte F, Fernandes JC, Martel-Pelletier J, Pelletier JP, Lajeunesse D. Modulation of insulin-like growth factor 1 levels in human osteoarthritic subchondral bone osteoblasts. Bone 2006 Mar;38(3):333–41.
16. Okazaki K, Jingushi S, Ikenoue T, Urabe K, Sakai H, Ohtsuru A, *et al*. Expression of insulin-like growth factor I messenger ribonucleic acid in developing osteophytes in murine experimental osteoarthritis and in rats inoculated with growth hormone-secreting tumor. Endocrinology 1999 Oct;140(10):4821–30.
17. Akatsu T, Takahashi N, Debari K, Morita I, Murota S, Nagata N, *et al*. Prostaglandins promote osteoclast like cell formation by a mechanism involving cyclic adenosine 3',5'-monophosphate in mouse bone marrow cell cultures. J Bone Min Res 1989 Feb;4(1):29–35.
18. McErlain DD, Ulici V, Darling M, Gati JS, Pitelka V, Beier F, *et al*. An in vivo investigation of the initiation and progression of subchondral cysts in a rodent model of secondary osteoarthritis. Arthritis Res Ther 2012 Feb 3;14(1):R26.
19. Zanetti M, Bruder E, Romero J, Hodler J. Bone marrow edema pattern in osteoarthritic knees: correlation between MR imaging and histologic findings. Radiology 2000 Jun;215(3):835–40.
20. Taljanovic MS, Graham AR, Benjamin JB, Gmitro AF, Krupinski EA, Schwartz SA, *et al*. Bone marrow edema pattern in advanced hip osteoarthritis: quantitative assessment with magnetic resonance imaging and correlation with clinical examination, radiographic findings, and histopathology. Skeletal Radiol 2008 May;37(5):423–31.
21. Xu L, Hayashi D, Roemer FW, Felson DT, Guermazi A. Magnetic resonance imaging of subchondral bone marrow lesions in association with osteoarthritis. Semin Arthritis Rheum 2012 Oct;42(2):105–18.

22. Crema MD, Roemer FW, Zhu Y, Marra MD, Niu J, Zhang Y, *et al*. Subchondral cystlike lesions develop longitudinally in areas of bone marrow edema-like lesions in patients with or at risk for knee osteoarthritis: detection with MR imaging–the MOST study. Radiology 2010 Sep;256(3):855–62.
23. Torres L, Dunlop DD, Peterfy C, Guermazi A, Prasad P, Hayes KW, *et al*. The relationship between specific tissue lesions and pain severity in persons with knee osteoarthritis. Osteoarthritis Cartilage 2006 Oct;14(10):1033–40.
24. Libicher M, Ivancic M, Hoffmann M, Wenz W. Early changes in experimental osteoarthritis using the pond-nuki dog model: technical procedure and initial results of in vivo MR imaging. Eur Radiol 2005 Feb;15(2):390–4.
25. Wang YX. In vivo magnetic resonance imaging of animal models of knee osteoarthritis. Lab Anim 2008 Jul;42(3):246–64.
26. Abduljalil AM, Robitaille PM. Macroscopic susceptibility in ultra high field MRI. J Comput Assist Tomogr 1999 Nov-Dec;23(6):832–41.
27. Appel H, Loddenkemper C, Grozdanovic Z, Ebhardt H, Dreimann M, Hempfing A, *et al*. Correlation of histopathological findings and magnetic resonance imaging in the spine of patients with ankylosing spondylitis. Arthritis Res Ther 2006;8(5):R143.
28. Altman R, Asch E, Bloch D, Bole G, Borenstein D, Brandt K, *et al*. Development of criteria for the classification and reporting of osteoarthritis. classification of osteoarthritis of the knee. Diagnostic and therapeutic criteria committee of the American rheumatism association. Arthritis Rheum 1986 Aug;29(8):1039–49.
29. Kerkhof HJ, Bierma-Zeinstra SM, Arden NK, Metrustry S, Castano-Betancourt M, Hart DJ, *et al*. Prediction model for knee osteoarthritis incidence, including clinical, genetic and biochemical risk factors. Ann Rheum Dis Published Online First: [2013 Aug 20]. http://dx.doi.org/10.1136/annrheumdis-2013-203620
30. Oehler S, Neureiter D, Meyer-Scholten C, Aigner T. Subtyping of osteoarthritic synoviopathy. Clin Exp Rheumatol 2002 Sep–Oct;20(5):633–40.
31. Sokolove J, Lepus CM. Role of inflammation in the pathogenesis of osteoarthritis: latest findings and interpretations. Ther Adv Musculoskelet Dis 2013 Apr;5(2):77–94.